SUPPLEMENT

THE MATERHORN

Unraveling the Intricacies of Mountain Weather

BY H. J. S. FERNANDO, E. R. PARDYJAK, S. DI SABATINO, F. K. CHOW, S. F. J. DE WEKKER, S. W. HOCH, J. HACKER, J. C. PACE, T. PRATT, Z. PU, J. W. STEENBURGH, C. D. WHITEMAN, Y. WANG, D. ZAJIC, B. BALSLEY, R. DIMITROVA, G. D. EMMITT, C. W. HIGGINS, J. C. R. HUNT, J. C. KNIEVEL, D. LAWRENCE, Y. LIU, D. F. NADEAU, E. KIT, B. W. BLOMQUIST, P. CONRY, R. S. COPPERSMITH, E. CREEGAN, M. FELTON, A. GRACHEV, N. GUNAWARDENA, C. HANG, C. M. HOCUT, G. HUYNH, M. E. JEGLUM, D. JENSEN, V. KULANDAIVELU, M. LEHNER, L. S. LEO, D. LIBERZON, J. D. MASSEY, K. MCENERNEY, S. PAL, T. PRICE, M. SGHIATTI, Z. SILVER, M. THOMPSON, H. ZHANG, AND T. ZSEDROVITS

This document is a supplement to "The MATERHORN: Unraveling the Intricacies of Mountain Weather," by H. J. S. Fernando, E. R. Pardyjak, S. Di Sabatino, F. K. Chow, S. F. J. De Wekker, S. W. Hoch, J. Hacker, J. C. Pace, T. Pratt, Z. Pu, J. W. Steenburgh, C. D. Whiteman, Y. Wang, D. Zajic, B. Balsley, R. Dimitrova, G. D. Emmitt, C. W. Higgins, J. C. R. Hunt, J. C. Knievel, D. Lawrence, Y. Liu, D. F. Nadeau, E. Kit, B. W. Blomquist, P. Conry, R. S. Coppersmith, E. Creegan, M. Felton, A. Grachev, N. Gunawardena, C. Hang, C. M. Hocut, G. Huynh, M. E. Jeglum, D. Jensen, V. Kulandaivelu, M. Lehner, L. S. Leo, D. Liberzon, J. D. Massey, K. McEnerney, S. Pal, T. Price, M. Sghiatti, Z. Silver, M. Thompson, H. Zhang, and T. Zsedrovits (*Bull. Amer. Meteor. Soc.*, **96**, 1945–1967) • ©2015 American Meteorological Society • Corresponding author: Harindra Joseph Fernando, Environmental Fluid Dynamics Laboratories, Department of Civil and Environmental Engineering and Earth Sciences and Department of Aerospace and Mechanical Engineering, University of Notre Dame, Notre Dame, IN 46556-5637 • E-mail: hfernand@nd.edu • DOI:10.1175/BAMS-D-13-00131.2

Additional collaborators:

Professors Ben Balsley* and Dale Lawrence, University of Colorado Boulder, Boulder, Colorado
Dr. David J. Gochis, National Center for Atmospheric Research, Boulder, Colorado
Professor Chad Higgins, Oregon State University, Corvallis, Oregon
Professor Marcus Hultmark, Princeton University, Princeton, New Jersey
Dr. Jason Knievel, National Center for Atmospheric Research, Boulder, Colorado
Professor Daniel F. Nadeau, École Polytechnique de Montréal, Montreal, Quebec, Canada
Professor Joachim Reuder, University of Bergen, Bergen, Norway
Dr. Dorita Rostkier-Edelstein, Environmental Sciences Division, IIBR, Ness Ziona, Israel
Dr. Stefano Serafin, University of Vienna, Vienna, Austria
Dr. Yansen Wang, U.S. Army Research Laboratory, Adelphi, Maryland

REFERENCES

Hocut, C. M., 2013: Multi-scale flow and turbulence in complex terrain under weak synoptic conditions. Ph.D. dissertation, University of Notre Dame, 163 pp.

* In memoriam.

Table ES1. Physical parameters for the main land use types of GMAST and surroundings.					
Site	Roughness height (m)	Average albedo		Soil thermal conductivity ($W\ m^{-1}\ K^{-1}$)	
		Oct	May	Oct	May
IOS-Playa	5.7×10^{-4}	0.31	0.34	0.98	0.79
IOS-Sagebrush	0.24	0.27	0.24	0.59	0.73
IOS-ES	0.10	0.23	0.19	0.44	0.54

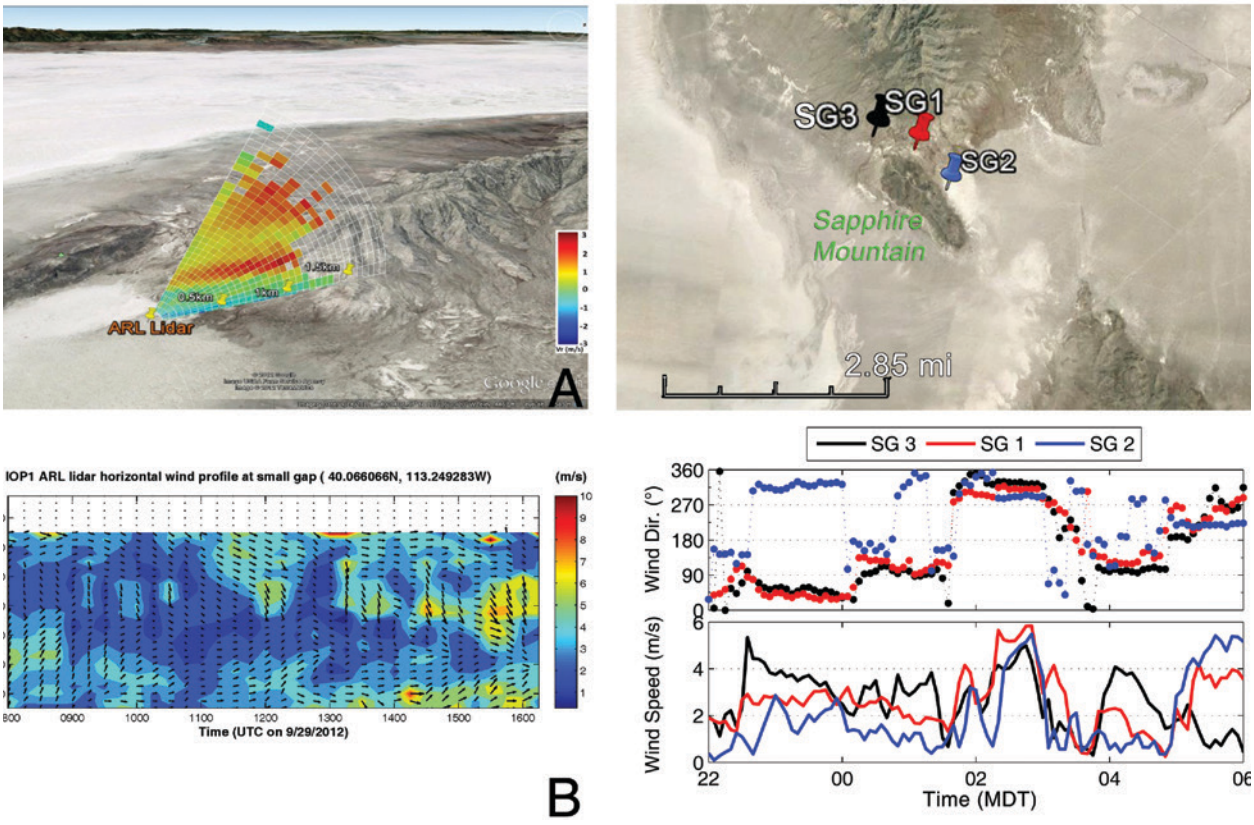

Fig. ES1. In the fall campaign, the lidar placement near the small gap allowed plan position indicator (PPI), range–height indicator (RHI), and velocity azimuth display (VAD) scans through and surrounding the gap. (a) When directed along the slope, lidar captured the downslope flow. (b) When aimed at a location in the gap, complex flow patterns with varying magnitude and direction were evident; see time–height plots. (c) For a closer look at the gap flow, in the spring campaign the small gap was instrumented with three towers: SG 1, SG 2, and SG 3. Tower data indicated how the competition between multiple flows and forcing mechanisms determine the spatiotemporal nature of gap flow. (d) In the early evening of a quiescent day (the night of 10 May), 10-m levels of SG 1 and SG 3 located on the northern bank of thalweg show (northeasterly) katabatic winds to the gap from GM although there is (northwesterly) drainage through the thalweg that passes though SG 2. Suddenly, around 0000 MDT, the SG 2 flow reverses, and SG 1 and SG 2 adjust so that drainage is easterly. After draining for an hour or so, SG 3 experiences a reversal, indicating strong horizontal shear in the gap, easterly flow in the northern banks, and northwesterly flow over the southern banks. Lapsed another half an hour or so, all towers show a stronger flow (strait flow!) from west to east basins. Such vacillations continue within a mesoscale grid point, which obviously cannot be resolved by canonical mesoscale models. These submesoscale processes are critical to the mountain weather prediction and point out the need for ultra-high-resolution modeling advocated in MATERHORN.

Table ES2. Details of instrumentation (from Hocut 2013).

Instrument	Quantity measured	Range[a]	Accuracy
100S Doppler lidar	U_r, SNR	Up to 12 km	<0.5 m s^{-1}
3D sonic anemometer	*U*, *V*, *W*, *T*	—	±0.05 m s^{-1}, ±2°C
Ceilometer	Cloud-height detection aerosol backscatter	0–7.6 km	±5 m
DataHawk unmanned aerial vehicles (UAV)[b]	*U*, *V*, *W*, *T*, CT^2, RH, *P*, ε	Up to 3 km AGL	0.1 m s^{-1}, 0.3°C, 1.0×10^{-6}, 0.01%, 1.0 Pa, 1.0×10^{-6} W kg^{-1}
Distributed temperature sensing (DTS) system[b]	T	2 km	±0.1°C
Fine-wire thermocouple	T	—	±0.2°C
Flamingo UAV[b]	*u*', *v*', *w*', ε, *T*, RH	12.8 km	4% for 30% TI
FLIR IR camera	~~T~~ ——	max FOV = 63.2° × 52.4°	±2°C or ±2%
Flux Richardson probe	$u'w'$ and $w'T'$	—	±10%
Frequency-modulated continuous-wave (FM-CW) radar	C_n^2	Usually set to 4 km	—
Gravimetric soil observations[c]	VWC	Surface and 5 and 25 cm below the surface	1%–3%
Heat flux plates	Soil *Q*	—	–15% to +5%
HMP45 probe	*T*, RH	—	±0.6°C, ±3%
HOBO U23 Pro v2	*T*, RH	—	±0.21°C, ±3.5%
Hot-film combo probe	*u*', *v*', *w*', ε	—	4% for 30% TI
Infrared gas analyzer	CO_2 and H_2O density	—	1% and 2%
Krypton hygrometer	H_2O vapor fluctuations	—	—
Local energy-balance measurement stations (LEMS)	*P*, *T*, RH, T_S, VWC_{soil}, T_{soil}, SW_i	—	±0.035 kPa, ±0.3°C, ±2%, ±2%, ±0.03 m^3 m^{-3}, ±1°C, ±3%
Levelogger Gold[c]	Water table depth	0–1 m below the surface	0.05% F.S.
Microwave radiometer profiler[c]	*T*, H_2O vapor ρ profie, liquid H_2O profile, derived RH	0–10 km	±2°C, ±0.5 g m^{-3}, 0.1 g m^{-3}, 20%
Mini-SoDAR	*U*, WD	50–400 m	0.5 m s^{-1}, ±2°
Net radiometer	SW_i, SW_o, LW_i, LW_o	—	±10%
Pyranometer (CMP21)	SW_i, SW_o	—	±5 W m^{-2}
Pyrgeometer (CGR4)	LW_i, LW_o	—	±10 W m^{-2}
Radiosonde	*T*, RH, *P*, *U*	Up to 30 km	0.5°C, 5%, 1 hPa, 0.2 m s^{-1}
RF polarimetric crosshair	Soil moisture	1-km grid scale	—

Table ES2. Continued.			
Instrument	**Quantity measured**	**Range[a]**	**Accuracy**
Sound detection and range/radio acoustic sounding system (SoDAR/RASS)	*U*, *W*, WD, *T*	30 m–1 km	<0.3 m s^{-1}, <0.1 m s^{-1}, ±1.5°, 0.2°C
Streamline Doppler lidar	U_r, SNR	Up to 10 km	<0.5 m s^{-1}
Tethersonde	*T*, RH, *P*, *U*, WD	0–500 m	0.5°C, 5%, 1.5 hPa, 0.1 m s^{-1}, 1°
TP01 soil property probe	Thermal conductivity	0.3–4 Wm^{-1} K^{-1}	±5%
Twin Otter Wind lidar (TODWL)[b]	*U*, *V*, *W*, SNR	0.3–21 km	<0.1 m s^{-1}
Wind monitor anemometer	*U*, WD	—	±0.3 m s^{-1}, ±3°
Wind Profiler 449	*U*, WD	0.075–16 km	±1 m s^{-1}, ±10°
Wind Profiler 924	*U*, WD	0.075–5 km	<1 m s^{-1}, <10°

[a] Represents the maximum possible range. Results depend on atmospheric conditions.

[b] Only present during the fall campaign.

[c] Only present during the spring campaign.

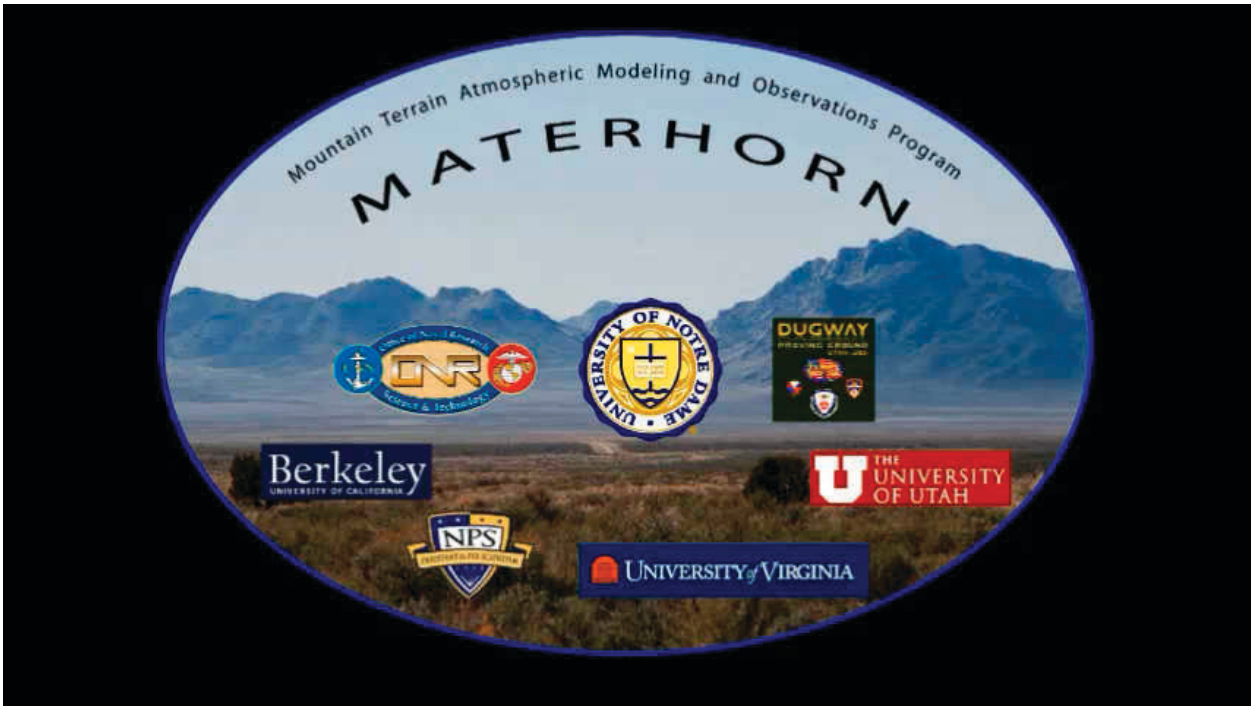

Fig. ES2. Movie on flow visualization (http://www3.nd.edu/~dynamics/materhorn/Media/LasVisGravCur.wmv**).**